J. Fluid Mech. (2010), vol. 648, pp. 471–484.
doi:10.1017/S0022112009994034

Scaling of decaying shallow axisymmetric swirl flows

M. DURAN-MATUTE†, L. P. J. KAMP, R. R. TRIELING AND G. J. F. VAN HEIJST

Department of Applied Physics and J. M. Burgers Centre, Eindhoven University of Technology, PO Box 513, 5600 MB Eindhoven, The Netherlands

(Received 16 July 2009; revised 1 December 2009; accepted 15 December 2009)

There is a lack of rigour in the usual explanation for the scaling of the vertical velocity of shallow flows based on geometrical arguments and the continuity equation. In this paper we show, by studying shallow axisymmetric swirl flows, that the dynamics of the flow are crucial to determine the proper scaling. In addition, we present two characteristic scaling parameters for such flows: $Re\delta^2$ for the radial velocity and $Re\delta^3$ for the vertical velocity, where Re is the Reynolds number of the swirl flow and $\delta = H/L$ is the flow aspect ratio with H the fluid depth and L a typical horizontal length scale. This scaling contradicts the common assumption that the vertical velocity should scale with the primary motion proportional to the aspect ratio δ. Moreover, if this scaling applies, then the primary flow can be considered as quasi-two-dimensional. Numerical simulations of a decaying Lamb–Oseen vortex served to test the analytical results and to determine their range of validity. It was found that the primary flow can be considered as quasi-two-dimensional only if $\delta Re^{1/2} \lesssim 3$ and $\delta Re^{1/3} \lesssim 1$.

1. Introduction

Experiments on shallow fluid layers generally serve to study quasi-two-dimensional flows as an approximation to fully two-dimensional flows. For example, experiments in an electromagnetically forced shallow layer of electrolyte showed good agreement with results of two-dimensional simulations and a theoretical study of two-dimensional flows (Tabeling *et al.* 1991). In addition, the inverse energy cascade and the process of self-organization, both characteristic of two-dimensional flows, were observed in similar experiments in a stratified two-layer configuration (Paret & Tabeling 1997). Furthermore, experiments on a horizontal turbulent impulsive jet have shown a preponderant influence of the layer depth on the flow dynamics. For deep flows, the jet remains fully three-dimensional and is not constrained by the boundaries. On the other hand, for shallow layers, the flow is characterized by a damping of the vertical motion and the formation of large-scale horizontal vortex structures, which is also characteristic of two-dimensional flows (Sous, Bonneton & Sommeria 2005).

It is commonly assumed that in shallow flows, the magnitude of the vertical velocity is constrained because of the small aspect ratio. This argument is derived from continuity of mass and is valid if the flow has vertical shear and is fully turbulent

† Email address for correspondence: m.duran.matute@tue.nl

(Jirka & Uijttewaal 2004). In Cartesian coordinates (x, y, z), the continuity equation for an incompressible fluid reads

$$\frac{\partial v_x}{\partial x} + \frac{\partial v_y}{\partial y} = -\frac{\partial v_z}{\partial z}, \tag{1.1}$$

where z is the vertical coordinate and $\boldsymbol{v} = (v_x, v_y, v_z)$ is the fluid velocity. If L is a typical horizontal scale of the flow, and H is a typical vertical scale, then (1.1) implies that

$$\frac{[v_x]}{L} \sim \frac{[v_y]}{L} \sim \frac{[v_z]}{H}, \tag{1.2}$$

where the brackets denote the order of magnitude of the enclosed quantity. Consequently,

$$[v_z] \sim \frac{H}{L}[v_x] \sim \frac{H}{L}[v_y]. \tag{1.3}$$

This suggests that for shallow flows ($H/L \ll 1$), the vertical velocities are much smaller than the horizontal velocities and that the ratio of vertical velocity to horizontal velocity scales with the aspect ratio $\delta = H/L$. Furthermore, this argument is used to neglect the vertical velocities in shallow flows and consider such flows as quasi-two-dimensional.

However, recent experiments in a shallow fluid layer have revealed vertical velocities higher than expected and complicated three-dimensional flow structures. For example, electromagnetically generated dipolar vortices have shown persistent three-dimensional structures and regions of high vertical velocities (Akkermans *et al.* 2008). Furthermore, vertical velocities did not scale proportional to H/L. Consequently, it was concluded that this shallow flow cannot be considered as quasi-two-dimensional.

In the current paper, we focus on shallow axisymmetric swirl flows like monopolar vortices, which are considered as the building blocks of quasi-two-dimensional turbulence. The flow, on top of a no-slip horizontal bottom, is initialized with a specific azimuthal velocity distribution and is subsequently left to freely evolve. It is well known that in such a swirling flow a secondary flow arises with both radial and vertical velocity components. Of particular interest is the scaling commonly used to quantify the degree of two-dimensionality of the flow of both the radial and vertical velocities with respect to the primary azimuthal motion.

The degree of two-dimensionality of a shallow axisymmetric monopolar vortex has been previously quantified in numerical simulations using three criteria based on (i) the ratio of the kinetic energies associated with the radial and the azimuthal velocity components, (ii) the ratio of the kinetic energies associated with the vertical and the azimuthal velocity components and (iii) the deformation of the vorticity profile as compared with the initial profile. It was found that the degree of two-dimensionality depends not only on the aspect ratio but also on the Reynolds number (Satijn *et al.* 2001). This explains partly why some shallow flows behave in a quasi-two-dimensional way, while some others do not, and it is also a sign that the scaling of the vertical velocity cannot be simply derived from geometrical arguments based on the continuity equation. Clearly, it is still not well understood why some shallow flows do not behave in a quasi-two-dimensional way.

In the current work, by expanding the velocity components in powers of the aspect ratio δ, we find at lowest order a simplified version of the axisymmetric Navier–Stokes equations for shallow swirl flows where advection and radial diffusion are

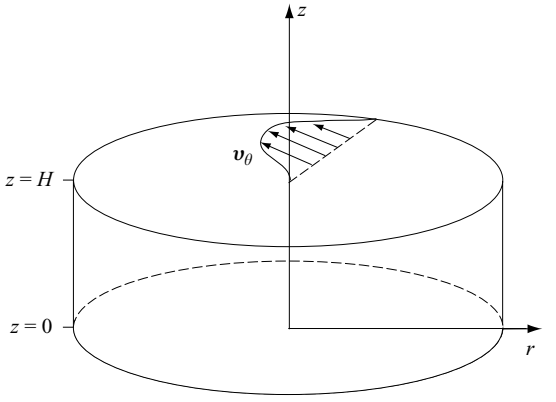

FIGURE 1. Sketch of the flow's geometry.

neglected. Then, these equations are solved analytically for a realistic initial azimuthal velocity profile. The analytical results are then compared with numerical simulations of the full axisymmetric Navier–Stokes equations. This allows us to derive the proper scaling for shallow axisymmetric flows and to find the range of validity for this scaling.

The paper is organized as follows: § 2 presents the governing equations and the geometry pertinent to the problem. In § 3, we present a perturbation approach leading in lowest order to a simplified Navier–Stokes equation that is solved analytically in § 4. Section 5 is devoted to the results from numerical simulations of a Lamb–Oseen monopolar vortex, which serve to quantify the range of validity of the analytical results. Finally, the conclusions are presented in § 6.

2. Governing equations and geometry

We consider a flow governed by the Navier–Stokes equations

$$\frac{\mathrm{D}\boldsymbol{v}}{\mathrm{D}t} = -\frac{1}{\rho}\nabla p + \nu\nabla^2\boldsymbol{v} \tag{2.1}$$

and the continuity equation for an incompressible fluid

$$\nabla\cdot\boldsymbol{v} = 0, \tag{2.2}$$

where $\mathrm{D}/\mathrm{D}t$ is the material derivative; $\boldsymbol{v}$ is the velocity; ν is the kinematic viscosity; p is the pressure; and ρ is the density of the fluid.

Since we are interested in axisymmetric swirl flows, it is convenient to use cylindrical coordinates (r, θ, z); the velocity is then written as $\boldsymbol{v} = (v_r, v_\theta, v_z)$ and the vorticity as $\boldsymbol{\omega} = \nabla\times\boldsymbol{v} = (\omega_r, \omega_\theta, \omega_z)$.

The fluid is vertically confined by a no-slip bottom ($\boldsymbol{v} = 0$ at $z = 0$) and a rigid, flat surface (at $z = H$) that is assumed to be stress free (see figure 1).

The flow is initialized with a particular axisymmetric azimuthal velocity profile $v_\theta(r, z, t = 0) \neq 0$ while $v_r(r, z, t = 0) = v_z(r, z, t = 0) = 0$; afterward, the flow is left to freely evolve.

3. Shallow-swirl-flow approximation

In order to non-dimensionalize the governing equations (2.1) and (2.2), we introduce the following non-dimensional variables denoted by the tildes:

$$\tilde{t} = \frac{\nu}{H^2}t, \qquad \tilde{r} = \frac{r}{L}, \qquad \tilde{z} = \frac{z}{H},$$
$$[\tilde{v}_\theta, \tilde{v}_r, \tilde{v}_z] = \frac{1}{U}[v_\theta, v_r, v_z], \qquad \tilde{\omega}_\theta = \frac{H}{U}\omega_\theta,$$

where U is a typical velocity scale of the flow.

Since we consider a flow with azimuthal symmetry ($\partial/\partial\theta = 0$), we can rewrite (2.1) and (2.2) in terms of $\tilde{v}_\theta$ and $\tilde{\omega}_\theta$, so that we obtain

$$\frac{\partial \tilde{v}_\theta}{\partial \tilde{t}} + Re\delta^2\left(\tilde{v}_r\frac{\partial \tilde{v}_\theta}{\partial \tilde{r}} + \frac{\tilde{v}_\theta\tilde{v}_r}{\tilde{r}}\right) + Re\delta\tilde{v}_z\frac{\partial \tilde{v}_\theta}{\partial \tilde{z}} = \delta^2\left[\frac{\partial^2\tilde{v}_\theta}{\partial\tilde{r}^2} + \frac{\partial}{\partial\tilde{r}}\left(\frac{\tilde{v}_\theta}{\tilde{r}}\right)\right] + \frac{\partial^2\tilde{v}_\theta}{\partial\tilde{z}^2}, \quad (3.1)$$

$$\frac{\partial \tilde{\omega}_\theta}{\partial \tilde{t}} + Re\delta^2\left(\tilde{v}_r\frac{\partial \tilde{\omega}_\theta}{\partial \tilde{r}} - \frac{\tilde{\omega}_\theta\tilde{v}_r}{\tilde{r}}\right) + Re\delta\tilde{v}_z\frac{\partial \tilde{\omega}_\theta}{\partial \tilde{z}} - Re\delta^2\frac{1}{\tilde{r}}\frac{\partial \tilde{v}_\theta^2}{\partial \tilde{z}}$$
$$= \delta^2\left[\frac{\partial^2\tilde{\omega}_\theta}{\partial\tilde{r}^2} + \frac{\partial}{\partial\tilde{r}}\left(\frac{\tilde{\omega}_\theta}{\tilde{r}}\right)\right] + \frac{\partial^2\tilde{\omega}_\theta}{\partial\tilde{z}^2}, \quad (3.2)$$

$$\delta\frac{1}{\tilde{r}}\frac{\partial}{\partial\tilde{r}}(\tilde{r}\tilde{v}_r) + \frac{\partial \tilde{v}_z}{\partial\tilde{z}} = 0, \quad (3.3)$$

$$\tilde{\omega}_\theta = \frac{\partial \tilde{v}_r}{\partial\tilde{z}} - \delta\frac{\partial \tilde{v}_z}{\partial\tilde{r}}, \quad (3.4)$$

with $\delta = H/L$ the aspect ratio and $Re = UL/\nu$ the Reynolds number. To simplify notation, the tildes will be omitted from here on.

Note that the continuity equation (3.3) does not provide any relation between the azimuthal velocity and the vertical velocity. Consequently, the scaling of the ratio of the azimuthal velocity to the vertical velocity must be determined by the flow dynamics.

In this context, the term

$$\frac{Re\delta^2}{r}\frac{\partial v_\theta^2}{\partial z} = \frac{2Re\delta^2}{r}v_\theta\frac{\partial v_\theta}{\partial z} \quad (3.5)$$

in (3.2) is of special interest, since it couples the azimuthal velocity v_θ with both the radial velocity v_r and the vertical velocity v_z, implying that a vertical gradient in v_θ will drive a secondary flow in the (r-z) plane

To study the limit of shallow flows ($\delta \ll 1$), we propose an asymptotic expansion of the variables in powers of δ:

$$\omega_\theta = \sum_{n=0}^{\infty}\delta^n\omega_{\theta,n}, \quad v_\theta = \sum_{n=0}^{\infty}\delta^n v_{\theta,n}, \quad v_r = \sum_{n=0}^{\infty}\delta^n v_{r,n}, \quad v_z = \sum_{n=0}^{\infty}\delta^n v_{z,n}. \quad (3.6)$$

By substituting (3.6) into (3.3), we immediately obtain that $v_{z,0} = 0$.

Substitution of (3.6) into (3.2) yields

$$\frac{\partial \omega_{\theta,0}}{\partial t} - \frac{\partial^2\omega_{\theta,0}}{\partial z^2} = 0 \quad (3.7)$$

at zeroth order,

$$\frac{\partial \omega_{\theta,1}}{\partial t} - \frac{\partial^2\omega_{\theta,1}}{\partial z^2} = 0 \quad (3.8)$$

at first order and

$$\frac{\partial \omega_{\theta,2}}{\partial t} + Re\left(v_{r,0}\frac{\partial \omega_{\theta,0}}{\partial r} + \frac{v_{r,0}\omega_{\theta,0}}{r} + v_{z,1}\frac{\partial \omega_{\theta,0}}{\partial z}\right) - Re\frac{1}{r}\frac{\partial v_{\theta,0}^2}{\partial z} = \frac{\partial^2 \omega_{\theta,0}}{\partial r^2} + \frac{\partial}{\partial r}r^{-1}\omega_{\theta,0} + \frac{\partial^2 \omega_{\theta,2}}{\partial z^2} \quad (3.9)$$

at second order.

Note, from (3.7) and (3.8), that $\omega_{\theta,0}$ and $\omega_{\theta,1}$ are not affected by the primary motion and only depend on the initial condition for ω_θ. In fact, if $v_r = v_z = 0$ at $t = 0$, then $\omega_{\theta,0} = \omega_{\theta,1} = 0$ and $v_{r,0} = v_{r,1} = v_{z,1} = v_{z,2} = 0$. Substituting these results into (3.9) yields

$$\frac{\partial \omega_{\theta,2}}{\partial t} - \frac{\partial^2 \omega_{\theta,2}}{\partial z^2} = Re\frac{1}{r}\frac{\partial v_{\theta,0}^2}{\partial z}. \quad (3.10)$$

It can be seen from this equation that a vertical gradient in v_θ will drive a secondary flow that at lowest order ($\delta \downarrow 0$) scales as follows:

$$\omega_\theta = \delta^2 \omega_{\theta,2}, \quad v_r = \delta^2 v_{r,2}, \quad v_z = \delta^3 v_{z,3}, \quad (3.11)$$

provided that $\omega_\theta = 0$ at $t = 0$. Therefore, it is convenient to define the new variables

$$\hat{\omega}_\theta = \frac{\omega_\theta}{\delta^2 Re}, \quad \hat{v}_r = \frac{v_r}{\delta^2 Re}, \quad \hat{v}_z = \frac{v_z}{\delta^3 Re}, \quad \hat{v}_\theta = v_\theta, \quad (3.12)$$

through which (3.1) and (3.2) simplify to

$$\frac{\partial \hat{v}_\theta}{\partial t} - \frac{\partial^2 \hat{v}_\theta}{\partial z^2} = 0, \quad (3.13)$$

$$\frac{\partial \hat{\omega}_\theta}{\partial t} - \frac{\partial^2 \hat{\omega}_\theta}{\partial z^2} = \frac{1}{r}\frac{\partial \hat{v}_\theta^2}{\partial z}, \quad (3.14)$$

where $\hat{\omega}$, $\hat{v}_r$, $\hat{v}_z$, $\hat{v}_\theta$ are all $O(1)$ for $\delta \downarrow 0$. This implies that the velocity components scale to lowest order as

$$\frac{v_r}{v_\theta} = O(Re\delta^2) \quad (3.15)$$

and

$$\frac{v_z}{v_\theta} = O(Re\delta^3). \quad (3.16)$$

If we consider the azimuthal velocity as the typical horizontal velocity – a common choice – the latter result contradicts the usual assumption that the ratio of vertical velocity to horizontal velocity should scale with δ. Not only does the vertical velocity scale with δ^3, but it also depends linearly on the Reynolds number of the primary motion. The range of validity for the scaling proposed in (3.15) and (3.16) will be studied using numerical simulations in § 5.

4. Analytical solution for a shallow swirl flow

Equation (3.13) is a diffusion equation, where both radial diffusion and advection by the secondary motion have been neglected as compared with (3.1). Since at lowest order the evolution of the main flow is independent of the secondary flow, flows governed by (3.13) and (3.14) can be considered as quasi-two-dimensional.

To analyse the two-dimensionality and the evolution of shallow swirl flows, (3.13) and (3.14) are solved analytically. For this, we consider as initial condition a swirl

flow with a Poiseuille-like vertical structure and a radial dependence which is, at this stage, arbitrary:

$$\hat{v}_\theta(r, z, 0) = R(r)\sin(\pi z/2), \tag{4.1}$$

where $R(r)$ is such that $\mathrm{d}R(r)/\mathrm{d}r$ is of the same order of magnitude as $R(r)$. This is achieved by choosing the appropriate radial length scale L. Furthermore, for the secondary motion we consider

$$\hat{\omega}_\theta(r, z, 0) = 0. \tag{4.2}$$

The Poiseuille-like vertical profile was used as initial condition, since the vertical structure of shallow axisymmetric vortices dominated by bottom friction tends quickly to such a profile (Satijn *et al.* 2001).

The solution of (3.13) that satisfies the no-slip boundary condition at the bottom ($\hat{v}_\theta = 0$ at $z = 0$), the stress-free boundary condition at the top ($\partial\hat{v}_\theta/\partial z = 0$ at $z = 1$) and the initial condition (4.1) is given by

$$\hat{v}_\theta(r, z, t) = R(r)\sin\left(\frac{\pi}{2}z\right)\exp\left(-\frac{\pi^2}{4}t\right). \tag{4.3}$$

We note that the azimuthal velocity $\hat{v}_\theta$ decays exponentially at a rate $\lambda_R = \pi^2/4$ ($\lambda'_R = (\pi^2\nu)/(4H^2)$ in dimensional form) which is, in some studies, referred to as the external friction parameter. For shallow flows, it is also known as the Rayleigh friction parameter, and it is commonly used to parameterize the vertical dependence of shallow flows in two-dimensional equations with a linear friction term (Dolzhanskii, Krymov & Manin 1992; Satijn *et al.* 2001).

By substituting (4.3) into (3.14), we obtain an equation for the secondary flow that is driven by the primary swirl:

$$\frac{\partial\hat{\omega}_\theta}{\partial t} - \frac{\partial^2\hat{\omega}_\theta}{\partial z^2} = \frac{\pi}{2}\frac{R(r)^2}{r}\sin(\pi z)\exp\left(-\frac{\pi^2}{2}t\right). \tag{4.4}$$

To solve (4.4) with the appropriate boundary conditions, it is useful to introduce the stream function $\hat{\psi}$ defined by

$$\hat{v}_r = -\frac{1}{r}\frac{\partial\hat{\psi}}{\partial z}, \tag{4.5}$$

$$\hat{v}_z = \frac{1}{r}\frac{\partial\hat{\psi}}{\partial r}. \tag{4.6}$$

From this and (3.4), $\hat{\omega}_\theta$ is given by

$$\hat{\omega}_\theta = -\frac{1}{r}\frac{\partial^2\hat{\psi}}{\partial z^2} - \delta^2\frac{\partial}{\partial r}\left(\frac{1}{r}\frac{\partial\hat{\psi}}{\partial r}\right) \tag{4.7}$$

which at lowest order ($\delta \downarrow 0$) reduces to

$$\hat{\omega}_\theta = -\frac{1}{r}\frac{\partial^2\hat{\psi}}{\partial z^2}. \tag{4.8}$$

The evolution of the secondary flow is now governed by the following equation:

$$\frac{\partial^4\Psi}{\partial z^4} - \frac{\partial}{\partial t}\frac{\partial^2\Psi}{\partial z^2} = \sin(\pi z)\exp\left(-\frac{\pi^2}{2}t\right), \tag{4.9}$$

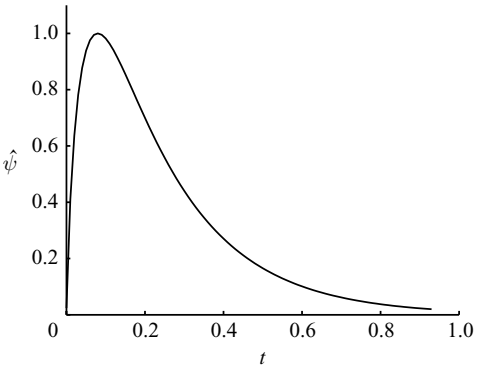

FIGURE 2. Normalized stream function as a function of time.

where

$$\Psi(z,t) = \frac{2}{\pi}\frac{\hat{\psi}(r,z,t)}{R^2(r)}, \tag{4.10}$$

with the boundary conditions

$$\Psi(0,t) = 0, \quad \Psi(1,t) = 0, \quad \left.\frac{\partial \Psi(z,t)}{\partial z}\right|_{z=0} = 0, \quad \left.\frac{\partial^2 \Psi(z,t)}{\partial z^2}\right|_{z=1} = 0 \tag{4.11}$$

and the initial condition

$$\Psi(z,0) = 0. \tag{4.12}$$

The detailed procedure to solve the initial-value problem (4.9)–(4.12) is given in the Appendix, and the solution is

$$\begin{aligned}\Psi(z,t) = {} & \frac{2\sin(\pi z)}{\pi^4}\mathrm{e}^{-\pi^2 t/2} \\ & + \frac{2}{\pi^3(\tan(\pi/\sqrt{2}) - \pi/\sqrt{2})}\left\{\tan\left(\frac{\pi}{\sqrt{2}}\right)\left[1 - z - \cos\left(\frac{\pi}{\sqrt{2}}z\right)\right] + \sin\left(\frac{\pi}{\sqrt{2}}z\right)\right\}\mathrm{e}^{-\pi^2 t/2} \\ & - \sum_{n=0}^{\infty}\frac{4\gamma_n}{\pi\tan^2(\gamma_n)(\pi^2 - \gamma_n^2)(\pi^2 - 2\gamma_n^2)}\left[\tan(\gamma_n)(1 - z - \cos(\gamma_n z)) + \sin(\gamma_n z)\right]\mathrm{e}^{-\gamma_n^2 t},\end{aligned} \tag{4.13}$$

where γ_n are solutions of the transcendental equation $\tan(\gamma_n) = \gamma_n$.

Figure 2 shows the temporal evolution of the normalized stream function at an arbitrary location in the (r-z) plane and which is characteristic for the overall behaviour of $\hat{\psi}$. Initially, the normalized stream function shows a rapid increase as the secondary motion is set up by the primary flow. During this transient period, the infinite series in (4.13) forms the dominant contribution to $\hat{\psi}$. For longer times, the behaviour of the secondary motion is dominated by the first and second terms on the right-hand side of (4.13) since $\pi^2/2 \ll \gamma_n^2$. Note that the second term is present in the solution because the first term alone does not satisfy the boundary condition at the no-slip bottom.

From the stream function $\hat{\psi}$, we can calculate both the radial and vertical velocity components,

$$v_r = -\frac{Re\delta^2}{r}\frac{\partial\hat{\psi}}{\partial z} = -\frac{\pi Re\delta^2}{2}\frac{R(r)^2}{r}\frac{\partial\Psi(z,t)}{\partial z}, \tag{4.14}$$

$$v_z = \frac{Re\delta^3}{r}\frac{\partial\hat{\psi}}{\partial r} = \frac{\pi Re\delta^3}{2r}\frac{\partial R(r)^2}{\partial r}\Psi(z,t), \tag{4.15}$$

which will be compared in the next section with results from numerical simulations.

5. Numerical study

Numerical simulations were performed to determine the range of validity of the analytical results presented in the preceding sections. A finite-element code (see Comsol AB 2009) was used to solve the full Navier–Stokes equations. The flow was assumed to be incompressible and azimuthally symmetric ($\partial/\partial\theta = 0$).

The initial azimuthal flow was taken to be

$$v_\theta(r, z, 0) = R(r)\sin\left(\frac{\pi}{2}z\right), \tag{5.1}$$

where the radial dependence was specified as

$$R(r) = \frac{1}{2r}[1 - \exp(-r^2)]. \tag{5.2}$$

Such vortex is known as a Lamb–Oseen vortex, and it was chosen because of its similarity to some vortices created in the laboratory (e.g. Hopfinger & van Heijst 1993). However, as shown in § 3, the scaling of v_r and v_z is independent of the radial profile for $\delta \downarrow 0$.

The computational domain extends in the (r-z) plane for $0 \leqslant r \leqslant 12$ and $0 \leqslant z \leqslant 1$. The radial length of the container is approximately 10 times the radius of maximum velocity of the Lamb–Oseen vortex and large enough to neglect the effects of this boundary on the secondary motion.

As boundary conditions, we applied axial symmetry at $r = 0$ and a stress-free condition at $r = 12$ to further reduce the influence of this lateral boundary. In the vertical, a stress-free condition was applied at $z = 1$ and a no-slip boundary condition at the bottom ($z = 0$). At the top boundary, a 'rigid-lid' approximation is implemented, so excluding free-surface deformations.

We performed simulations at Reynolds number $Re = 100$, 1000 and 2500 where the typical velocity U is defined as $U = L\omega_0$, with ω_0 the maximum of the vertical vorticity component at $t = 0$. In addition, for each Re value the aspect ratio δ was varied within the range $1 \leqslant \delta^2 Re \leqslant 160$.

To study the scaling of the velocity components, we define the kinetic energy for each velocity component v_i (where $i = r, \theta, z$) as

$$E_i = \pi\int_0^1\int_0^{12} v_i^2 r\,\mathrm{d}r\,\mathrm{d}z \tag{5.3}$$

and the kinetic energy ratio of each velocity component v_i as

$$q_i = \frac{E_i}{E_\theta}. \tag{5.4}$$

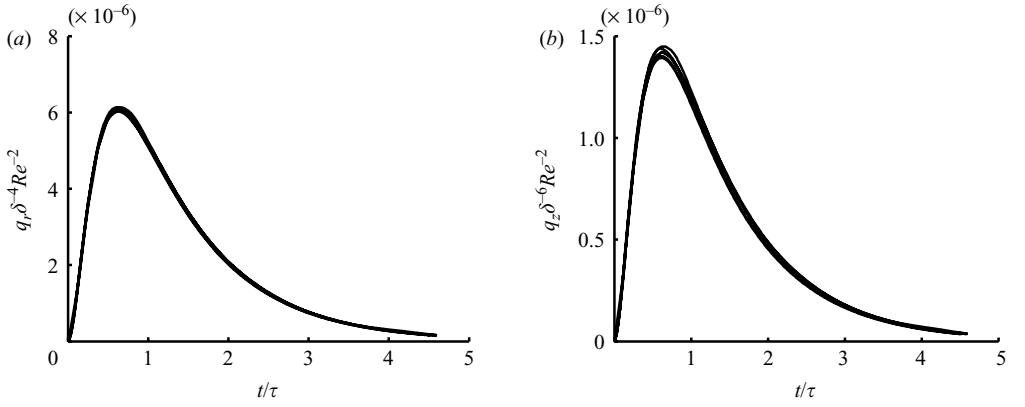

FIGURE 3. (*a*) Kinetic energy ratio $q_r/\delta^4 Re^2$ as a function of time for $Re = 1000$, 2500 and $\delta^2 Re = 1, 2, 5$. (*b*) Kinetic energy ratio $q_z/\delta^6 Re^2$ as a function of time for $Re = 1000$, 2500 and $\delta^2 Re = 1, 2, 5$. Time is normalized with $1/\lambda$.

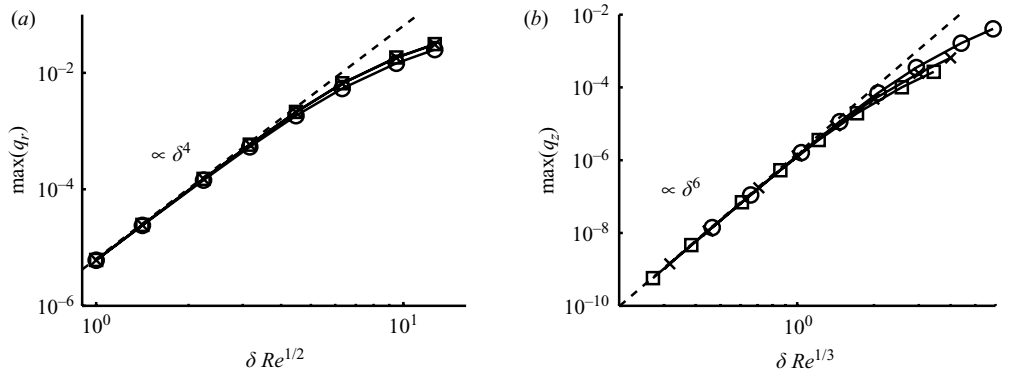

FIGURE 4. Values of (*a*) $\max(q_r)$ as a function of $\delta Re^{1/2}$ and (*b*) $\max(q_z)$ as a function of $\delta Re^{1/3}$ for $Re = 100$ (circles), $Re = 1000$ (crosses) and $Re = 2500$ (squares). The dashed line represents the analytical solution given by (4.3), (4.14) and (4.15).

In addition, a typical decay rate λ for each numerical solution is obtained by fitting the exponential function $\exp(-2\lambda t)$ to E_θ.

Figure 3 shows (*a*) the value of $q_r/(Re^2\delta^4)$ and (*b*) the value of $q_z/(Re^2\delta^6)$ as a function of time for $Re = 1000$, 2500 and $\delta^2 Re = 1, 2, 5$. Clearly, the six curves collapse to one curve in each graph. This means that the evolution of q_r is self-similar when scaling q_r with $(\delta^2 Re)^2$ for $\delta^2 Re = 1$, 2, 5 and that the evolution of q_z is self-similar when scaling q_z with $(\delta^3 Re)^2$ for the same values $\delta^2 Re = 1$, 2, 5. This is consistent with the analytical solution obtained in the previous section (see (4.14) and (4.15)) for $\delta \downarrow 0$.

To quantify the range of validity of the observed self-similarity, we now focus on characteristic values of the quantities q_r and q_z, namely $\max(q_r)$ and $\max(q_z)$.

Figure 4(*a*) shows the maximum value of the kinetic energy associated with the radial velocity, i.e. $\max(q_r)$, for simulations with $Re = 100$, 1000 and 2500 as a function of $\delta Re^{1/2}$ together with the results obtained from the analytical expressions (4.3), (4.14) and (4.15). As can be seen, for $\delta Re^{1/2} \lesssim 3$, the numerical results coincide well with the analytical solution; hence, $\max(q_r)$ scales like $\delta^4 Re^2$. For larger values of $\delta Re^{1/2}$,

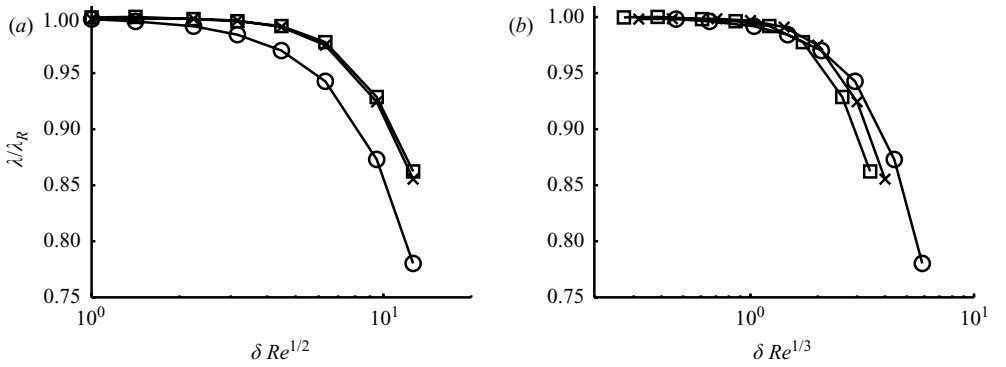

FIGURE 5. (*a*) The typical decay time λ/λ_R as a function of $\delta Re^{1/2}$ and (*b*) λ/λ_R as a function of $\delta Re^{1/3}$ for simulations with $Re = 100$ (circles), $Re = 1000$ (crosses) and $Re = 2500$ (squares).

there is a change in the slope of the curve given by the numerical results. For high Re values (e.g $Re = 1000, 2500$), this change in the slope is due to the increasing importance of advection. However, for these large Re values the results tend to the same curve, suggesting that the radial velocity only depends on $Re\delta^2$. On the other hand, for low Re values (e.g. $Re = 100$), the numerical results show a larger change in the slope. This can be explained since the aspect ratio is not small, and hence, horizontal diffusion cannot be neglected, and the approximation (4.8) does not hold.

The results obtained so far are reminiscent of the flow in curved pipes studied initially by Dean (1927). In such a flow there are two characteristic parameters: a geometrical parameter $\delta_D = a/R_D$, where a is the radius of the pipe and R_D is the radius of curvature of the pipe; and a dynamical quantity, the Reynolds number Re_D. Following this analogy, a straight pipe would be equivalent to an axisymmetric flow in a plane where, in both cases, no secondary motion exists. Furthermore, a loosely coiled pipe ($\delta_D \ll 1$) corresponds to a shallow flow $\delta \ll 1$. Dean (1927) expanded the Navier–Stokes equation in powers of δ_D and found that for $\delta_D \ll 1$ only one parameter $\kappa = \delta_D^{1/2} Re_D$ – known now as the Dean number – governs the flow. This gives rise to the so-called Dean number similarity. As found in the present paper, the governing parameter for shallow axisymmetric flows is $Re^2\delta$.

The graph in figure 4(*b*) shows the maximum of the kinetic energy associated with the vertical velocity, i.e. $\max(q_z)$, for simulations with $Re = 100,\ 1000$ and 2500 as a function of $\delta Re^{1/3}$ together with the analytical results given by (4.3), (4.14) and (4.15). As can be seen, for small values of $\delta Re^{1/3}$, the values of $\max(q_z)$ agree with the analytical results, indicating that the vertical velocity scales with $\delta^3 Re$. This contradicts the usual assumption that the vertical velocity scales with δ. However, this scaling breaks down for $\delta Re^{1/3} \gtrsim 1$ because of the effects of the advection associated with the secondary motion in the (r-z) plane.

Finally, we show how the change of regimes in the scaling of v_r and v_z relates to the primary motion and hence to the two-dimensionality of the flow. Figure 5 presents the decay parameter λ of the primary flow normalized by the Rayleigh parameter $\lambda_R = \pi^2/4$ as a function of (*a*) $\delta Re^{1/2}$ and (*b*) $\delta Re^{1/3}$. For $Re = 1000,\ 2500$ and $\delta Re^{1/2} \leqslant 3$, it is observed that $\lambda/\lambda_R \approx 1$, suggesting that (4.3) is valid in this regime. However, λ/λ_R starts to deviate strongly from unity for $\delta Re^{1/2} \approx 3$, which corresponds with the value of $\delta Re^{1/2}$ where the scaling of $\max(q_r)$ starts to deviate from the analytically obtained results for the secondary motion. For $Re = 100$, λ/λ_R deviates from unity for smaller values of $\delta Re^{1/2}$ than for $Re = 1000,\ 2500$. This is

due to the damping related to the horizontal momentum diffusion, which becomes important for large δ-values.

The deviation of λ from λ_R is related to qualitative changes in the azimuthal flow. For small values of $Re\delta^2$, the flow has a Poiseuille-like vertical structure. However, for large values of $Re\delta^2$, the flow consists of a thin boundary layer at the bottom and an inviscid interior. This is very similar in flows in curved pipes, where for small Dean number the main flow through the pipe is of Poiseuille type, while for large Dean number the flow is composed of a thin boundary layer and an inviscid core (Berger, Talbot & Yao 1983).

As shown in figure 5(*b*), for $\delta Re^{1/3} \lesssim 1$, $\lambda/\lambda_R \approx 1$ for all Re values. However, for $\delta Re^{1/3} \gtrsim 1$, it is observed that λ/λ_R deviates strongly from unity. Note that $\delta Re^{1/3} \approx 1$ is also the value of $\delta Re^{1/3}$ for which $\max(q_z)$ starts to strongly deviate from the analytical results. This suggests that for $\delta Re^{1/3} \gtrsim 1$ the secondary motion strongly affects the primary azimuthal flow and hence that the secondary motion cannot be neglected.

6. Discussion and conclusions

Using a formal perturbation approach in the aspect ratio δ, we obtained at lowest order ($\delta \downarrow 0$) a set of simplified Navier–Stokes equations for the evolution of a shallow axisymmetric swirl flow over a no-slip bottom. Flows governed by these simplified equations can be considered as quasi-two-dimensional, since the secondary motion can be neglected in the evolution of the primary azimuthal motion.

It was shown that for shallow axisymmetric swirl flows dominated by bottom friction the radial velocity scales with $\delta^2 Re$, while the vertical velocity scales with $\delta^3 Re$ with respect to the primary motion. Consequently, we conclude that the dynamics of the flow play a crucial role in the scaling of the vertical velocity and that the argument based only on the continuity equation is inadequate to explain this scaling. However, this argument seems to become valid for large values of $Re\delta^2$, i.e. when the shear flow is fully turbulent as considered by Jirka & Uijttewaal (2004). This can be seen in figure 4 since the value of $\max(q_r)$ tends towards being independent of δ for such large values of $Re\delta^2$. Nevertheless, we wish not to expand this work towards a fully turbulent case, since such regime should be treated differently.

Numerical simulations served to test the analytical results and to determine their range of validity. We compared the results from full three-dimensional numerical simulations of a decaying Lamb–Oseen vortex with the analytical solution of the simplified Navier–Stokes equations obtained for shallow swirl flows where advection due to the secondary flow has been neglected. Good agreement between the numerical and analytical solutions was found for $\delta Re^{1/2} \lesssim 3$ and $\delta Re^{1/3} \lesssim 1$. Consequently, for these values of $\delta Re^{1/2}$ and $\delta Re^{1/3}$ this flow can be considered as quasi-two-dimensional.

To quantify the two-dimensionality of shallow flows is a complicated matter. One quantity commonly used is the ratio of kinetic energy of the vertical velocity component to the kinetic energy of the horizontal velocity components. For example, Satijn *et al.* (2001) considered this ratio together with two other characteristic quantities and argued that the flow can be considered as quasi-two-dimensional if these quantities are smaller than a certain threshold, which is rather arbitrary. Another way to quantify the two-dimensionality of shallow flows is to estimate the dynamical forces related to the vertical or secondary motions. In this case, it is not *a priori* obvious whether these dynamical forces should be evaluated at a certain

location in the fluid or need to be averaged over a certain domain (see e.g. Akkermans *et al.* 2008). Hence, arbitrariness also exits depending on the position at which these forces are evaluated.

The regime in which the primary flow can be considered as quasi-two-dimensional is rarely studied in shallow-layer experiments. For example, experiments of a shallow electromagnetically driven dipolar vortex (Akkermans *et al.* 2008) were performed for $4 \lesssim \delta Re^{1/3} \lesssim 7.7$ and $Re \sim 4800$. Clercx, van Heijst & Zoeteweij (2003) performed experiments of quasi-two-dimensional turbulence in a shallow layer with a lower bound for $\delta Re^{1/3} \approx 2.17$ with $Re \approx 2500$. These experiments fall outside the range where $v_z/v_\theta = O(\delta^3 Re)$. Therefore, we propose experiments to be performed in the parameter regime studied in the current paper.

Even though the scaling proposed in the present paper is limited to the particular case of axisymmetric swirl flows, it is expected that it also applies to more complex flows, such as dipolar vortices and quasi-two-dimensional turbulence, since monopolar vortices can be considered as their building blocks. Research in this direction is still to be carried out.

M. D. M. gratefully acknowledges financial support from CONACYT (Mexico).

Appendix. Analytical solution

To solve (4.9), we perform a Laplace transform ($\mathscr{L}$) yielding

$$\frac{\partial^4 \bar{\Psi}}{\partial z^4} - s\frac{\partial^2 \bar{\Psi}}{\partial z^2} = \frac{2\sin(\pi z)}{2s + \pi^2}, \tag{A 1}$$

where $\bar{\Psi} = \mathscr{L}(\Psi)$. This equation has a solution of the form $\bar{\Psi} = \bar{\Psi}_h + \bar{\Psi}_p$, where

$$\bar{\Psi}_h(z, s) = A + B\pi z + C\sinh(\sqrt{s}z) + D\cosh(\sqrt{s}z) \tag{A 2}$$

is a solution of the homogeneous equation, with A, B, C and D being integration constants, and

$$\bar{\Psi}_p(z, s) = \frac{2\sin(\pi z)}{\pi^2(s + \pi)(2s + \pi)} \tag{A 3}$$

is a particular solution of (A 1).

Equations (A 2) and (A 3) give the following expression for the Laplace transform of the stream function:

$$\bar{\Psi}(z, s) = A + B\pi z + C\sinh(\sqrt{s}z) + D\cosh(\sqrt{s}z) + \frac{2\sin(\pi z)}{\pi^2(s + \pi)(2s + \pi)}. \tag{A 4}$$

Applying the boundary condition yields

$$\Psi(0, t) = A + D = 0, \tag{A 5}$$

$$\left.\frac{\partial \Psi(z, t)}{\partial z}\right|_{z=0} = B\pi + C\sqrt{s} + \frac{2}{\pi^2(\pi^2 + s)(\pi^2 + 2s)} = 0, \tag{A 6}$$

$$\Psi(1, t) = A + B\pi + C\sinh(\sqrt{s}) - A\cosh\sqrt{s} = 0 \tag{A 7}$$

and

$$\left.\frac{\partial^2 \Psi(z, t)}{\partial z^2}\right|_{z=1} = sC\sinh(\sqrt{s}) - sA\cosh(\sqrt{s}) = 0. \tag{A 8}$$

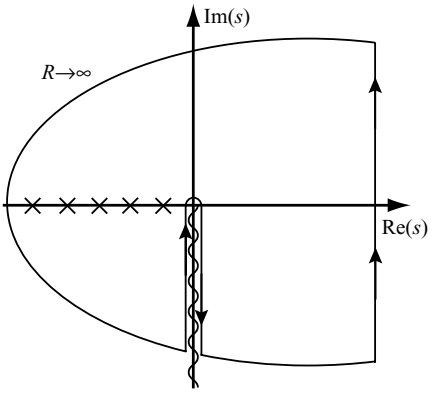

FIGURE 6. Integration contour for (A 13). The crosses in the real-s axis denote the poles.

Then, by combining (A 5)–(A 8), we obtain

$$C = -\frac{2}{\pi^2(\pi+s)(2s+\pi)}\frac{1}{\tanh(\sqrt{s})-\sqrt{s}}, \tag{A 9}$$

$$B = -\frac{2\tanh(\sqrt{s})}{\pi^3(\pi+s)(2s+\pi)}\frac{1}{\tanh(\sqrt{s})-\sqrt{s}} \tag{A 10}$$

and

$$A = -D = \frac{2}{\pi^2(\pi+s)(2s+\pi)}, \tag{A 11}$$

so that

$$\bar{\Psi}(z,s) = \frac{2}{\pi^2(\pi^2+s)(\pi^2+2s)} \times \left(\frac{1}{\tanh(\sqrt{s})-\sqrt{s}}\{\tanh(\sqrt{s})[1-z-\cosh(\sqrt{s}z)]+\sinh(\sqrt{z})\}+\sin(\pi z)\right). \tag{A 12}$$

The stream function Ψ can be recovered by inverting the Laplace transform, i.e.

$$\Psi(z,t) = \frac{1}{2\pi\mathrm{i}}\int_{c-\mathrm{i}\infty}^{c+\mathrm{i}\infty}\bar{\Psi}(z,s)\mathrm{e}^{st}\,\mathrm{d}s, \tag{A 13}$$

where c is to the right of all the singularities of $\bar{\Psi}$. These singularities are at $s=\pi^2/2$ and $s=\pi^2$, which are simple poles, and at $s=-\gamma_n^2$, where γ_n are solutions of the transcendental equation $\tan(\gamma_n)=\gamma_n$.

We perform the integration (A 13) in the complex s-plane along the contour of figure 6 which has a branch cut at $s=2\rho^2\exp(3\mathrm{i}\pi/2)$. However, it can be shown that this branch cut does not contribute to the integral and that

$$\Psi(z,t) = \frac{1}{2\pi\mathrm{i}}\int_{c-\mathrm{i}\infty}^{c+\mathrm{i}\infty}\bar{\Psi}(z,s)\mathrm{e}^{st}\,\mathrm{d}s = \sum \text{residues}. \tag{A 14}$$

REFERENCES

AKKERMANS, R. A. D., KAMP, L. P. J., CLERCX, H. J. H. & VAN HEIJST, G. J. F. 2008 Intrinsic three-dimensionality in electromagnetically driven shallow flows. *Europhys. Lett.* **83**, 24001.

Berger, S. A., Talbot, L. & Yao, L.-S. 1983 Flow in curved pipes. *Annu. Rev. Fluid Mech.* **15**, 461–512.

Clercx, H. J. H., van Heijst, G. J. F. & Zoeteweij, M. L. 2003 Quasi-two-dimensional turbulence in shallow fluid layers: the role of bottom friction and fluid layer depth. *Phys. Rev.* E **67**, 066303.

Comsol AB 2009 Comsol 3.5, User's Guide. Tegnérgatan 23, SE-111 40 Stockholm, Sweden. http://www.comsol.com.

Dean, W. R. 1927 XVI. Note on the motion of fluid in a curved pipe. *Phil. Mag. Ser.* 7 **4**, 208–223.

Dolzhanskii, F. V., Krymov, V. A. & Manin, D. Yu. 1992 An advanced experimental investigation of quasi-two-dimensional shear flows. *J. Fluid Mech.* **241**, 705–722.

Hopfinger, E. J. & van Heijst, G. J. F. 1993 Vortices in rotating fluids. *Annu. Rev. Fluid Mech.* **25**, 241–289.

Jirka, G. H. & Uijttewaal, W. S. J. 2004 Shallow flows: a definition. In *Shallow Flows* (ed. G. H. Jirka & W. S. J. Uijttewaal), pp. 3–11. Taylor & Francis.

Paret, J. & Tabeling, P. 1997 Experimental observation of the two-dimensional inverse energy cascade. *Phys. Rev. Lett.* **79**, 4162–4165.

Satijn, M. P., Cense, A. W., Verzicco, R., Clercx, H. J. H. & van Heijst, G. J. F. 2001 Three-dimensional structure and decay properties of vortices in shallow fluid layers. *Phys. Fluids* **13**, 1932–1945.

Sous, D., Bonneton, N. & Sommeria, J. 2005 Transition from deep to shallow water layer: formation of vortex dipoles. *Eur. J. Mech* B **24**, 19–32.

Tabeling, P., Burkhart, S., Cardoso, O. & Willaime, H. 1991 Experimental study of freely decaying two-dimensional turbulence. *Phys. Rev. Lett.* **67**, 3772–3775.